RESEARCH ARTICLE

Cancer-Stimulated Mesenchymal Stem Cells Create a Carcinoma Stem Cell Niche via Prostaglandin E_2 Signaling

Hua-Jung Li[1], Ferenc Reinhardt[1], Harvey R. Herschman[4], and Robert A. Weinberg[1-3]

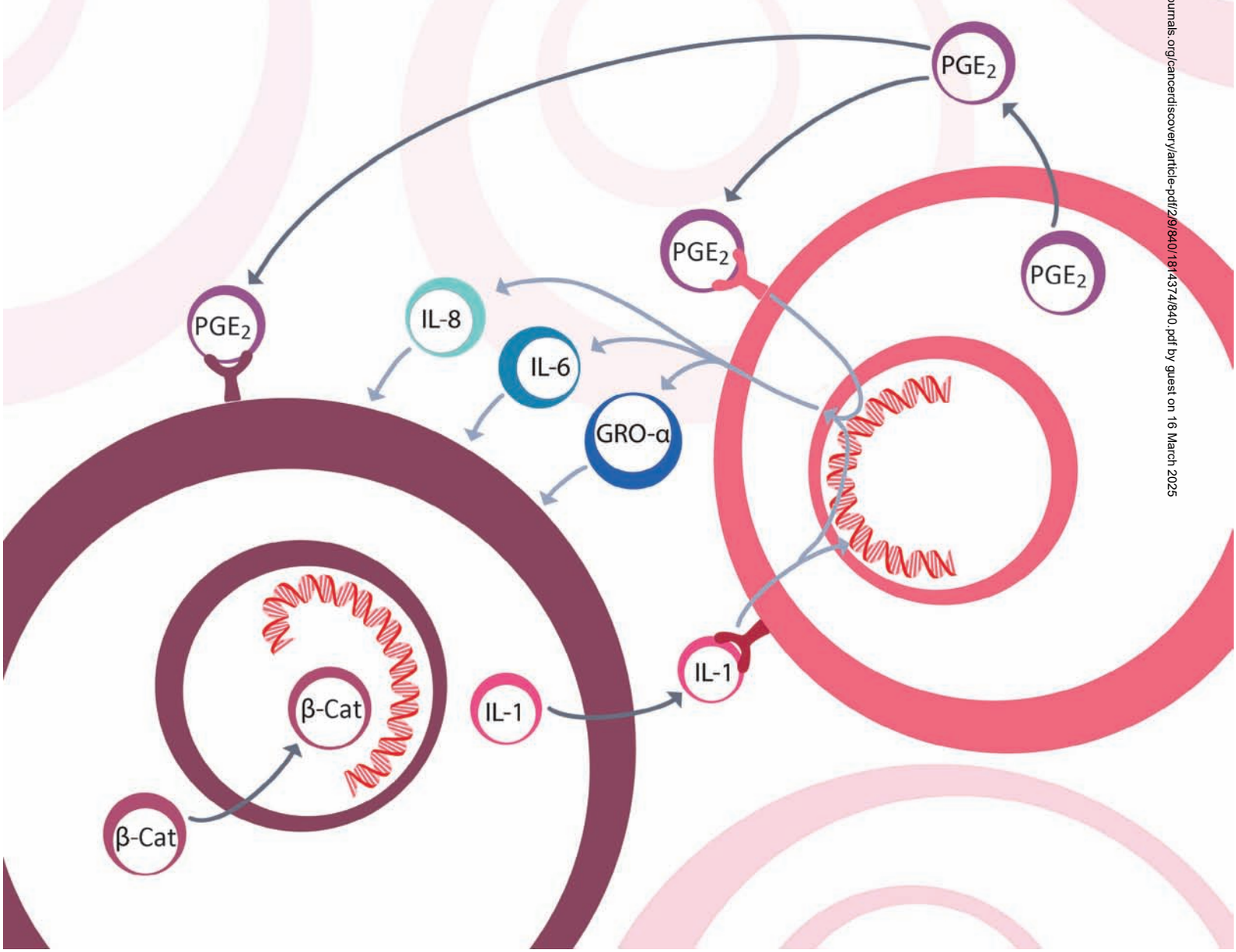

ABSTRACT

Mesenchymal cells of the tumor-associated stroma are critical determinants of carcinoma cell behavior. We focus here on interactions of carcinoma cells with mesenchymal stem cells (MSC), which are recruited to the tumor stroma and, once present, are able to influence the phenotype of the carcinoma cells. We find that carcinoma cell–derived interleukin-1 (IL-1) induces prostaglandin E_2 (PGE_2) secretion by MSCs. The resulting PGE_2 operates in an autocrine manner, cooperating with ongoing paracrine IL-1 signaling, to induce expression of a group of cytokines by the MSCs. The PGE_2 and cytokines then proceed to act in a paracrine fashion on the carcinoma cells to induce activation of β-catenin signaling and formation of cancer stem cells. These observations indicate that MSCs and derived cell types create a cancer stem cell niche to enable tumor progression via release of PGE_2 and cytokines.

SIGNIFICANCE: Although PGE_2 has been implicated time and again in fostering tumorigenesis, its effects on carcinoma cells that contribute specifically to tumor formation are poorly understood. Here we show that tumor cells are able to elicit a strong induction of the COX-2/microsomal prostaglandin-E synthase-1 (mPGES-1)/PGE_2 axis in MSCs recruited to the tumor-associated stroma by releasing IL-1, which in turn elicits a mesenchymal/stem cell–like phenotype in the carcinoma cells. *Cancer Discov; 2(9); 840–55. ©2012 AACR.*

INTRODUCTION

Carcinoma cells recruit mesenchymal cells into the tumor-associated stroma; these mesenchymal cells then proceed to modify the stroma, helping to establish a tissue microenvironment that favors tumor progression. Paracrine signals emanating from the resulting tumor-associated stroma can subsequently modulate the behavior of the carcinoma cells (1).

Among the recruited stromal cells are bone marrow–derived mesenchymal stem cells (MSC), which are known to exhibit multipotent differentiation potential (2). In the context of cancer pathogenesis, MSCs contribute to the formation of fibroblast and myofibroblast populations in the tumor-associated stroma (3, 4) and promote the growth, progression, and metastasis of tumors (3, 5, 6). Precisely how MSCs influence tumor progression is, however, poorly understood.

Elevated COX-2 mRNA and protein levels are found in many malignant tissues and are often associated with poor clinical outcome (7). The tumor-enhancing effects of COX-2 are generally ascribed to its role in producing prostaglandin E_2 (PGE_2), which has pleiotropic effects on cell proliferation, survival, angiogenesis, motility, and invasiveness (8). In addition to the neoplastic cells themselves, cells of the tumor-associated stroma contribute to elevated COX-2 expression (9, 10). However, it has been unclear whether the PGE_2 that promotes tumor progression derives from neoplastic cells, fibroblasts, macrophages, or some combination of these cell types.

Independent of these questions is the issue of heterogeneity of the neoplastic cells within carcinomas. Observations of a variety of human cancer types have revealed the existence of tumor-initiating cells (TIC), often called cancer stem cells (CSC), which coexist as minority populations within tumors, together with a majority population of cancer cells that lack tumor-initiating ability (11). Passage by neoplastic epithelial cells through an epithelial–mesenchymal transition (EMT) allows these cells to approach the stem cell state (12, 13). Moreover, EMT programs are known to be induced by heterotypic signals that epithelial cells receive from the microenvironment (14). However, the nature of these heterotypic signals and the identities of the stromal cells that release them remain poorly understood.

We show here that, in response to stimulation by carcinoma cells, MSCs express greatly elevated levels of PGE_2. The resulting PGE_2, together with cytokines also induced in the MSCs, contribute to entrance of nearby carcinoma cells into a stem cell–like state.

RESULTS

PGE_2 Induction in MSCs following Interaction with Carcinoma Cells

We initially studied the interactions in culture of LoVo and SW1116 human colorectal carcinoma cells with MSCs. Minimal PGE_2 accumulation was observed in pure LoVo, SW1116, or MSC cultures monitored over a 72-hour period (Fig. 1Aa and Supplementary Fig. S1A). However, PGE_2 levels increased by approximately 6.5-fold when the LoVo cells were cocultured with twice the number of MSCs for 48 hours and increased by approximately 60-fold after 72 hours of coculture. Correspondingly, levels of the COX-2 enzyme were

Authors' Affiliations: [1]Whitehead Institute for Biomedical Research; [2]Department of Biology, Massachusetts Institute of Technology; [3]MIT Ludwig Center for Molecular Oncology, Cambridge, Massachusetts; and [4]Departments of Biological Chemistry and Pharmacology, Molecular Biology Institute, and Jonsson Comprehensive Cancer Center, UCLA, Los Angeles, California

Note: Supplementary data for this article are available at Cancer Discovery Online (http://cancerdiscovery.aacrjournals.org/).

Corresponding Author: Robert A. Weinberg, Whitehead Institute for Biomedical Research, 9 Cambridge Center, Cambridge, MA 02142. Phone: 617-258-5159; Fax: 617-258-5230; E-mail: weinberg@wi.mit.edu

doi: 10.1158/2159-8290.CD-12-0101

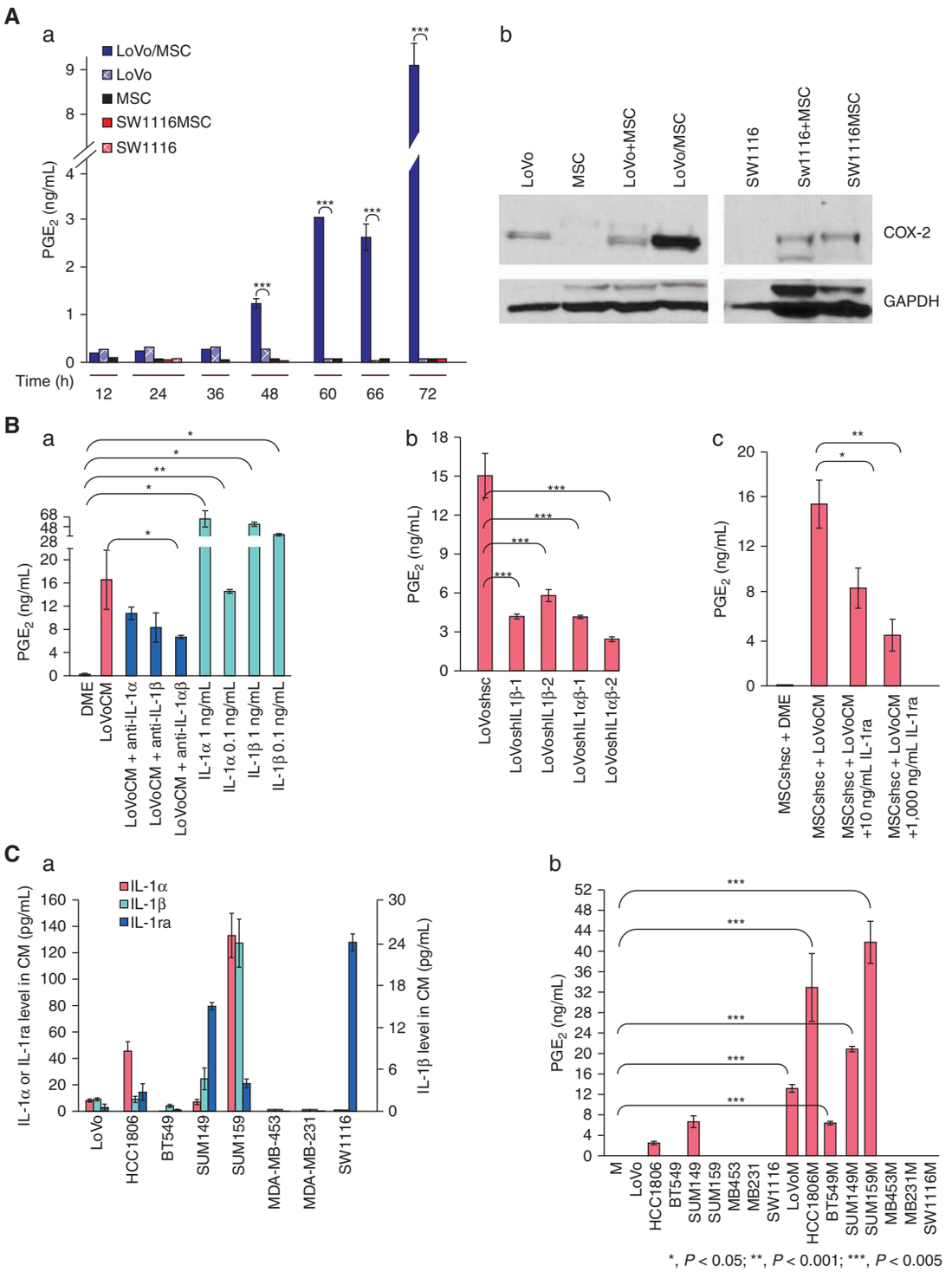

Figure 1. Carcinoma cell–secreted IL-1 induces PGE_2 production in MSCs. **A,** PGE_2 (a) and COX-2 (b) were measured in the indicated conditioned medium or cultures. PGE_2 data are means ± SE, $n = 3$. ***, $P < 0.005$ (vs. that in LoVo medium). LoVo + MSC; LoVo lysate and MSC lysate mixed in equal amounts; LoVo/MSC, lysate of LoVo/MSC coculture. The same nomenclature applies to the SW1116 cells. **B,** a, MSCs were treated with LoVoCM, LoVoCM with neutralizing antibodies (500 ng/mL), or IL-1 only. b, MSCs were cocultured with LoVo cells expressing shRNAs against IL1α + IL1β (LoVoshIL1αβ-1, LoVoshIL1αβ-2), IL1β (LoVoshIL1β-1, LoVoshIL1β-2), or a scrambled sequence (LoVoshsc).c, MSCs were treated with DME, LoVoCM, or LoVoCM+IL-1ra. After incubation, media were collected and assayed for PGE_2. Data are means ± SE, $n = 3$. **C,** a, IL-1α, IL-1β, and IL-1ra protein levels in conditioned medium of the carcinoma cells. Data are means ± SE, $n = 3$. b, PGE_2 levels in carcinoma cells, MSCs (M), and cocultures of the carcinoma cells with MSCs. Data are means ± SE, $n = 3$. ***, $P < 0.005$ (vs. that in MSC culture).

also increased in the coculture (Fig. 1Ab). In contrast, there was no PGE_2 increase in SW1116/MSC cocultures. Of note, PGE_2 production was induced equally strongly in [LoVo][MSC] transwell cocultures, which only permitted their intercommunication via soluble factors (Supplementary Fig. S1B) and in MSCs treated with LoVo-conditioned medium (LoVoCM; Supplementary Fig. S1C and S1D). Hence, soluble factors secreted by LoVo cells were responsible for inducing PGE_2 production by MSCs.

Other work (in Supplementary Data, Section 1; Supplementary Fig. S1E) showed that the secretion of interleukin-1β (IL-1β) and IL-1α by carcinoma cell populations was correlated with their respective abilities to elicit PGE_2 production in cocultured MSCs. Thus, when MSCs were treated with recombinant IL-1β or IL-1α, the induced PGE_2 levels were similar to or higher than those induced by LoVoCM (Fig. 1Ba). Conversely, IL-1α– and IL-1β–neutralizing antibodies attenuated by 60% the production of LoVoCM-induced PGE_2 (Fig. 1Ba). In addition, short hairpin RNAs (shRNA) directed against IL-1α and IL-1β mRNAs expressed in LoVo cells decreased by 84% the ability of their conditioned media to induce PGE_2 in MSCs (Fig. 1Bb) and recombinant IL-1ra, a natural antagonist of the IL-1 receptor, attenuated by 73% the LoVoCM-induced PGE_2 production by MSCs (Fig. 1Bc). IL-1 α/β secreted by the carcinoma cells was largely responsible for the PGE_2 production by MSCs, whereas IL-1ra could antagonize this induction.

Relationship of IL-1 Production by Carcinoma Cells to Their Ability to Induce PGE_2

The levels of the IL-1α, IL-1β, and IL-1ra mRNAs and secreted proteins were quantified in 6 human breast carcinoma cell lines and the SW1116 colorectal carcinoma cell line, in addition to the LoVo cells examined above. Cells of the LoVo, HCC1806, BT549, SUM149, and SUM159 lines expressed elevated levels of IL-1α and/or IL-1β, but relatively low levels of IL-1ra; conversely, MDA-MB-453, MDA-MB-231, and SW1116 cells secreted little or no detectable IL-1α/β and/or relatively high levels of IL-1ra (Supplementary Fig. S1F and Fig. 1Ca).

When cultured individually, the carcinoma cell lines expressed low or undetectable PGE_2 levels (Fig. 1Cb). However, upon coculture with MSCs, the IL-1α/β–secreting carcinoma cells induced approximately 80- to 500-fold increases of COX-2 and PGE_2 production, whereas the carcinoma cells secreting low levels of IL-1α/β failed to stimulate COX-2 or PGE_2 formation (Supplementary Fig. S1G and Fig. 1Cb). In addition, IL-1α-/IL-1β–neutralizing antibodies and IL-1ra attenuated PGE_2 production induced in MSCs by the conditioned media from the various IL-1–secreting carcinoma cells (Supplementary Fig. S1H). Hence, the ability to stimulate PGE_2 in MSCs seemed to be a frequent but not universal property of breast and colon carcinoma cells and was directly correlated with their abilities to signal via secreted IL-1α/β. Because IL-1α and IL-1β were both capable of PGE_2 induction, we used the term "IL-1" to refer to both IL-1α and IL-1β in the text that follows.

Induction of Cytokines in MSCs following Their Interaction with Carcinoma Cells

In addition to PGE_2, GRO-α, IL-6, IL-8, and regulated upon activation, normal T-cell expressed, and secreted (RANTES) in the culture media of LoVo/MSC cocultures increased by 34-, 10-, 79-, and 21-fold, respectively, following 120 hours of coculture (Fig. 2A). In [LoVo][MSC] transwell cultures, in which direct contact between the LoVo cells and MSCs was prevented, PGE_2, GRO-α, IL-6, and IL-8 were induced to comparable levels; in contrast, RANTES expression was not elevated (Fig. 2A). Following direct coculture, RANTES production occurred far more rapidly than did the accumulation of the other cytokines or PGE_2 (Supplementary Fig. S2A).

We also found that GRO-α, IL-6, and IL-8, like PGE_2, were induced by LoVoCM in MSCs (Supplementary Fig. S1B). To determine whether IL-1 was able, by itself, to induce concomitant production in MSCs of the 3 cytokines and PGE_2, we assessed mRNAs levels in MSCs that had been treated for 48 hours with vehicle or recombinant IL-1 (Fig. 2B). The resulting 10-fold and 4-fold increases in MSCs of COX-2 and microsomal prostaglandin-E synthase-1 [mPGES-1 (a second PGE_2 biosynthetic enzyme)] mRNAs, the increase of COX-2 protein, and the 10- to 100-fold decrease of 15-hydroxyprostaglandin dehydrogenase (15-PGDH) mRNA (encoding the PGE_2-degrading enzyme) confirmed the key role of IL-1 in modulating the levels of enzymes governing PGE_2 production and accumulation in MSCs. Moreover, IL-1 treatment alone elicited substantial increases (36- to 440-fold) of IL-6, IL-8, and GRO-α mRNAs in MSCs. COX-2, IL-6, IL-8, and GRO-α mRNA induction was detectable within 30 minutes of IL-1 exposure and reached a maximum at 1 to 2 hours thereafter (Supplementary Fig. S2B). This key role of IL-1 was further confirmed by knocking down IL-1α/β mRNAs in LoVo cells, resulting in a 60% to 90% decrease in the induced levels of IL-6, IL-8, and GRO-α mRNAs (Supplementary Fig. S2C). Thus, IL-1 was both necessary and sufficient to induce PGE_2, IL-6, IL-8, and GRO-α production in MSCs.

We also confirmed that LoVoCM and IL-1 could induce comparable levels of PGE_2 (Supplementary Fig. S2D) and cytokines (Supplementary Fig. S2E) in other types of mesenchymal cells that may arise from the differentiation of MSCs (4), including human breast MSCs (bMSCs) isolated from a breast cancer patient, human colonic myofibroblasts (CCD-18co), and primary human mammary stromal fibroblasts.

Autocrine PGE_2 Cooperation with IL-1 Paracrine Signaling Leading to PGE_2 and Cytokine Production by MSCs

IL-8 and IL-6 are known to be induced in certain cells by PGE_2 (15). To determine whether PGE_2 played a role in the induction of these cytokines in MSCs, PGE_2 production by MSCs was blocked with indomethacin, which inhibits the COX-1 and COX-2 enzymes. In LoVo/MSC cocultures, GRO-α, IL-6, and IL-8 protein induction was reduced by 85% to 98% by indomethacin; moreover, this induction could be partially rescued by providing PGE_2 to indomethacin-treated cocultures (Fig. 2C). Although PGE_2 treatment alone could not induce GRO-α, IL-6, or IL-8 expression in LoVo cells or MSC cells, additional PGE_2 potentiated the cytokine induction in LoVo/MSC cocultures and in IL-1–treated MSCs (Fig. 2C and Supplementary Fig. S2F).

MSCs expressed 2 distinct PGE_2 cell-surface receptors, EP2 and EP4 (Supplementary Fig. S2G). To support the notion that MSC-derived PGE_2 acted in an autocrine fashion, the EP2 and EP4 receptor antagonists AH6809 and GW627368X were added to MSC cultures, along with either LoVoCM

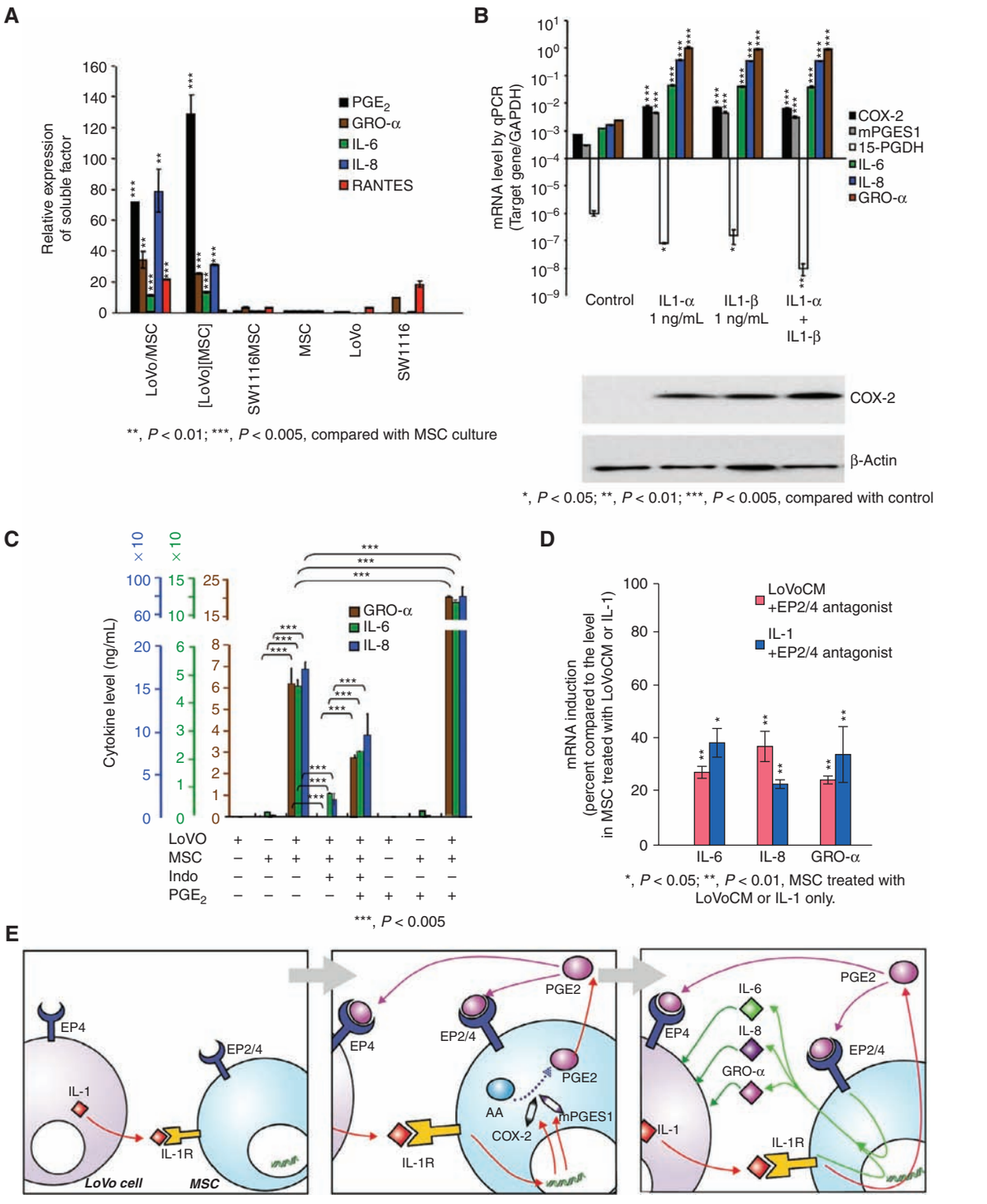

Figure 2. IL-1 and PGE_2 mediate GRO-α, IL-6, and IL-8, but not RANTES induction in carcinoma cell–MSC coculture. **A,** levels of PGE_2 and the cytokines were measured in conditioned media from the cultures. Data are means ± SE, $n = 3$. **, $P < 0.01$; ***, $P < 0.005$ (vs. that in MSC culture). **B,** mRNA levels of the enzymes governing PGE_2 production and the cytokines (top) and COX-2 protein levels (bottom) in MSCs treated with IL-1 as indicated. Data are means ± SE, $n = 3$. *, $P < 0.05$; **, $P < 0.01$; ***, $P < 0.005$ (vs. control). **C,** cytokine levels in conditioned media from MSCs, LoVo cells, and LoVo/MSC cocultures, in the presence of indomethacin (indo; 100 μmol/L), PGE_2 (100 nmol/L), or Indo + PGE_2. Data are means ± SE, $n = 3$. **D,** IL-6, IL-8, and GRO-α mRNA induction in MSCs either by LoVoCM or by IL-1 in the presence of EP2 and EP4 antagonists (AH6809 15 μmol/L + GW627368X 20 μmol/L). mRNA levels are set as 0% for vehicle-treated MSCs and 100% for LoVoCM-treated or IL-1–treated MSCs. Data are means ± SE, $n = 3$. *, $P < 0.05$; **, $P < 0.01$ (vs. MSC treated with LoVoCM or IL-1 without inhibitors). **E,** the proposed interactions for PGE_2 and cytokine induction from MSCs. AA, arachidonic acid.

or IL-1. LoVoCM- and IL-1–induced IL-6, IL-8, and GRO-α mRNA was suppressed by 60% to 80% by these EP receptor antagonists (Fig. 2D). Figure 2E summarizes our model that (i) COX-2, mPGES1, and PGE_2 are initially induced in MSCs by IL-1 released by carcinoma cells and that (ii) the resulting PGE_2, acting in an autocrine manner on MSCs, then cooperates with ongoing IL-1 paracrine signaling to trigger IL-6, IL-8, and GRO-α production by MSCs (Fig. 2E).

Effects of MSCs on Carcinoma Cell Mesenchymal and Invasive Traits

Before further analyzing the interactions between the carcinoma cells and MSCs, we confirmed that, as reported by others (5, 16), MSCs are indeed recruited to IL-1–secreting tumors *in vivo* (described in Supplementary Data, Section 2; Supplementary Fig. S3A and B). Having done so, we further investigated the influence of MSCs on carcinoma cell behavior, more specifically by analyzing the effects of MSC coculture on the expression by the tumor cells of markers of EMT, a cell–biological program that imparts motility, invasiveness, and self-renewal to carcinoma cells (14). After culturing, either alone or together with tandem dimer (td) Tomato-MSCs (5 days), LoVo and HCC1806 cells were isolated by fluorescence-activated cell sorting (FACS) and analyzed for E-cadherin, vimentin, fibronectin, and β-actin protein expression (Fig. 3A). E-cadherin, a key epithelial marker, was decreased by 98% to 100% in both LoVo and HCC1806 cells cocultured with MSCs. Conversely, vimentin and fibronectin proteins—both mesenchymal markers—were robustly induced in both carcinoma cells (Fig. 3A). Moreover, expression of the SNAIL protein, an EMT-inducing transcription factor (EMT-TF), was increased 5- to 69-fold in the MSC/carcinoma cocultures (Fig. 3A).

We then determined whether PGE_2 and/or the cytokines produced by MSCs in LoVo/MSC cocultures could elicit an EMT-like response in LoVo cells. PGE_2 was able, on its own, to cause a decrease in E-cadherin protein in LoVo cells (Fig. 3B, ~70% decrease) but failed to elicit concomitant robust increases of mesenchymal markers, that is, vimentin and the ZEB1, SNAIL, and TWIST1 EMT-TFs (Fig. 3B).

In contrast to PGE_2, IL-6 alone induced ZEB1 (7-fold), SNAIL (3-fold), and vimentin (3-fold) protein expression in LoVo cells, but was unable to decrease E-cadherin protein. However, treatment of LoVo cells with PGE_2 together with the 4 cytokines induced both a decrease of E-cadherin protein expression (~80%) and increases of vimentin (9-fold), ZEB1 (14-fold), SNAIL (13-fold), and TWIST1 (10-fold) protein expression (Fig. 3B). Hence, activation of a more complete EMT program in the carcinoma cells required the concomitant activation of multiple signaling pathways, specifically those triggered in these cells by PGE_2 acting together with the indicated cytokines.

Significantly more carcinoma cells invaded in LoVo/MSC cultures than in cultures of LoVo cells alone (Fig. 3C). To examine whether PGE_2 played a critical role in the MSC-induced carcinoma cell invasiveness, LoVo/MSC cocultures were treated with NS398, a COX-2 inhibitor; this treatment resulted in an 80% reduction of MSC-induced LoVo cell invasiveness (Fig. 3C). Greater than 60% of this inhibition could be reversed by adding PGE_2 to these cocultures.

Also, LoVo cell invasion was significantly reduced by antibodies that neutralize either IL-6, GRO-α, or RANTES (Fig. 3D). Accordingly, the MSC-induced carcinoma cell invasiveness seemed to derive from a confluence of PGE_2, IL-6, GRO-α, and RANTES signals impinging on the LoVo cells.

We also examined possible effects of MSCs on carcinoma cell invasion *in vivo*. The carcinoma cells injected on their own formed reasonably well-encapsulated tumors (Fig. 3E, a, b, c). In contrast, the carcinoma cells coinjected with MSCs formed extensive invasive fronts that extended into adjacent muscle layers (Fig. 3E, d, e, f). In addition, we observed the intravasation of carcinoma cells into nearby microvessels (Fig. 3E, insert). To summarize, these data indicated that MSCs facilitated LoVo cell invasion both *in vitro* and *in vivo*.

Effects of MSCs on Tumor Initiation by Carcinoma Cells

Due to the fact that transformed epithelial cells that have undergone EMT contain larger subpopulations of TICs (12, 13, 17), we determined whether EMT induction of carcinoma cells by MSCs was similarly accompanied by an increase in tumor-initiating ability. When populations of 5×10^4 IL-1–secreting carcinoma cells were coinjected with 2×10^5 MSCs, their ability to give rise to palpable tumors was measurably increased (1/6 to 6/6 for LoVo, 1/6 to 6/6 for HCC1806, 0/6 to 5/6 for SUM159 and 1/6 to 5/6 for SUM149, Fig. 3F). In contrast, tumor initiation by 5×10^4 MDA-MB-231 or MDA-MB-453 cells, neither of which secrete IL-1, was not increased by coinjection with 2×10^5 MSCs.

We quantified these interactions more precisely by implanting limiting dilutions of LoVo cells at 4 dosages, together with 5×10^5 admixed MSCs. The presence of admixed MSCs increased the tumor-initiating frequencies of 5×10^5, 5×10^4, and 5×10^3 implanted LoVo cells from 4/6, 1/6, and 0/6 to 6/6, 6/6, and 6/6. (Fig. 3G). As judged by the extreme limiting dilution analysis [ELDA (18)], the frequency of TICs in cultured LoVo cells was 9×10^{-7} to 6×10^{-5}; in the presence of admixed MSCs, this frequency increased to 1×10^{-3} to 1×10^{-2} (Fig. 3H).

MSC-Induced Increases in $ALDH^{high}$ CSC-Enriched Population and Tumor Initiation

CSCs, which have some characteristics associated with normal stem cells, are cells defined operationally by their tumor-initiating ability (19). We validated the use of aldehyde dehydrogenase (ALDH) as a marker of tumor-initiating cells and thus CSCs (refs. 20, 21; described in Supplementary Data, Section 3; Supplementary Figs. S4A–S4C and S5A–S5B). We observed that a 5-day coculture of LoVo or HCC1806 cells with MSCs resulted in approximately 7-fold and 20-fold increases, respectively, in ALDH1 protein levels in the carcinoma cells (Fig. 4A and Supplementary Fig. S5C). To extend this observation, we cultured an unfractionated LoVo cell population or already sorted $ALDH^{high}$ or $ALDH^{low}$ LoVo cell subpopulations (Supplementary Fig. S4Ba), either alone or in the presence of a 2-fold excess of tdTomato-labeled MSCs, for 5 days. All 3 LoVo cell populations, when cocultured with MSCs, developed larger subpopulations of $ALDH^{high}$ cells (59%, 38%, and 18%) than when cultured

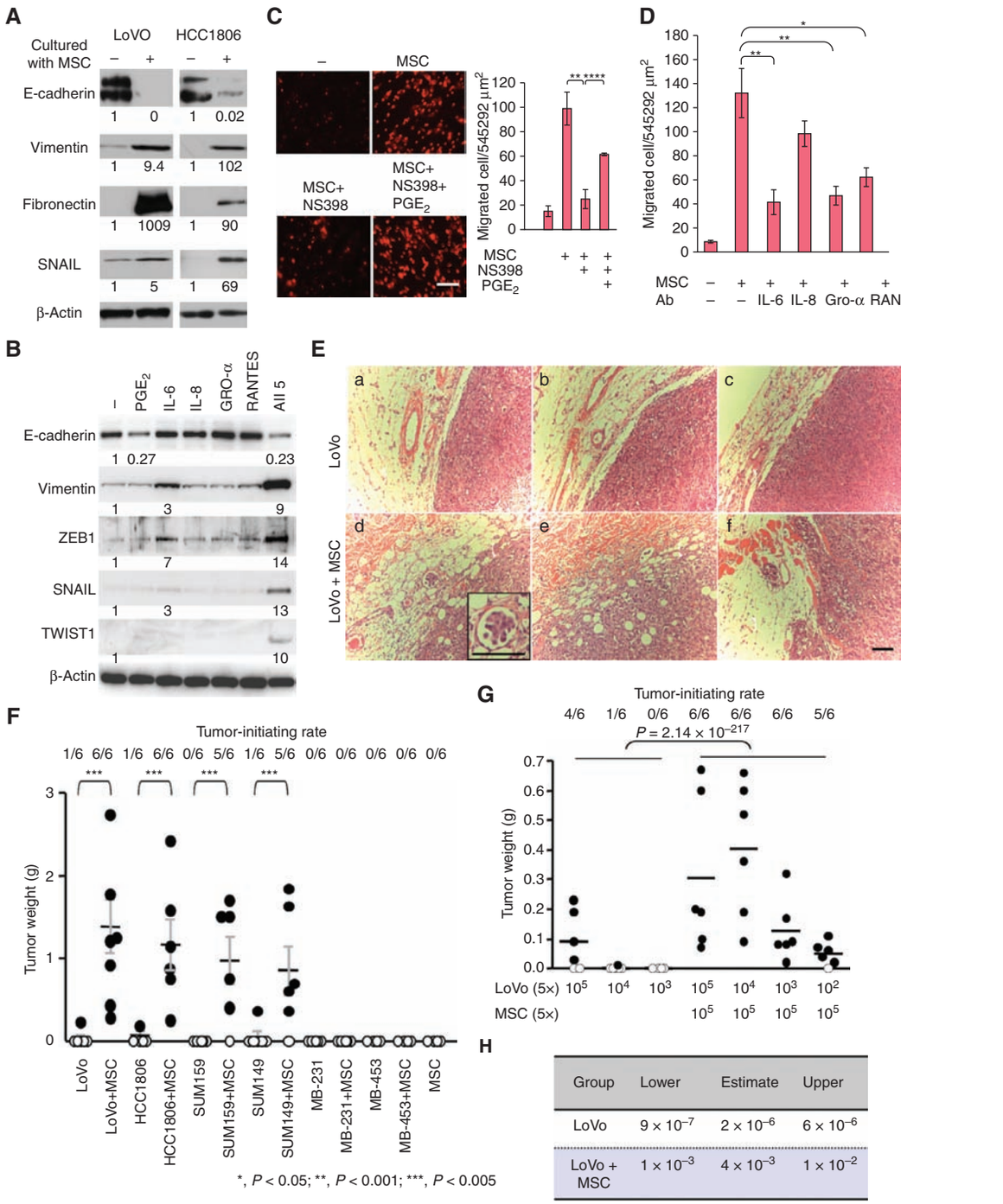

Figure 3. MSCs elicit EMT, invasion of carcinoma cells, and increased tumor initiation of xenografts. **A,** E-cadherin, vimentin, fibronectin, SNAIL, and β-actin protein expression in carcinoma cells cultured either alone or with MSCs. The numbers indicate relative protein levels. **B,** EMT markers and EMT-TFs were measured in LoVo cells treated with vehicle, PGE_2 (100 nmol/L), or the cytokines (100 ng/mL IL-6, 100 ng/mL IL-8, 100 ng/mL GRO-α, and/or 10 ng/mL RANTES) as indicated for 6 days. **C,** left: LoVo-tdTomato cells were cultured either alone or with MSCs in the upper wells of Boyden chambers. The presence or absence of NS398 (50 μmol/L) or NS-398 + PGE_2 (100 nmol/L) is indicated for each panel. The images show the LoVo-tdTomato cells that migrated through the Matrigel-coated membranes in 72 hours. Scale bar, 100 μm. Right, data are means ± SE, $n = 3$. **D,** LoVo cell migration in LoVo/MSC coculture treated with cytokine-neutralizing antibodies (Ab) as indicated. Data are means ± SE, $n = 5$. **E,** MSCs increase invasion of LoVo tumors. LoVo cells (5×10^5 cells per injection) were injected subcutaneously into SCID mice either alone (a, b, c) or with MSCs (5×10^5 cells per injection, d, e, f). After 8 weeks, tumors of comparable size were isolated. Hematoxylin and eosin staining was carried out on the tumor sections. Scale bar, 100 μm. **F** and **G,** weights of tumors derived from (**F**) carcinoma cells (5×10^4 cells per injection) and (**G**) LoVo cells injected into SCID mice, either alone or with MSCs. Filled circles indicate individual tumor weights; open circles indicate no tumor grew at the site of injection. Bars are means ± SE. **H,** the ranges of the estimated tumor-initiating frequencies in panel G evaluated by ELDA (with 95% confidence).

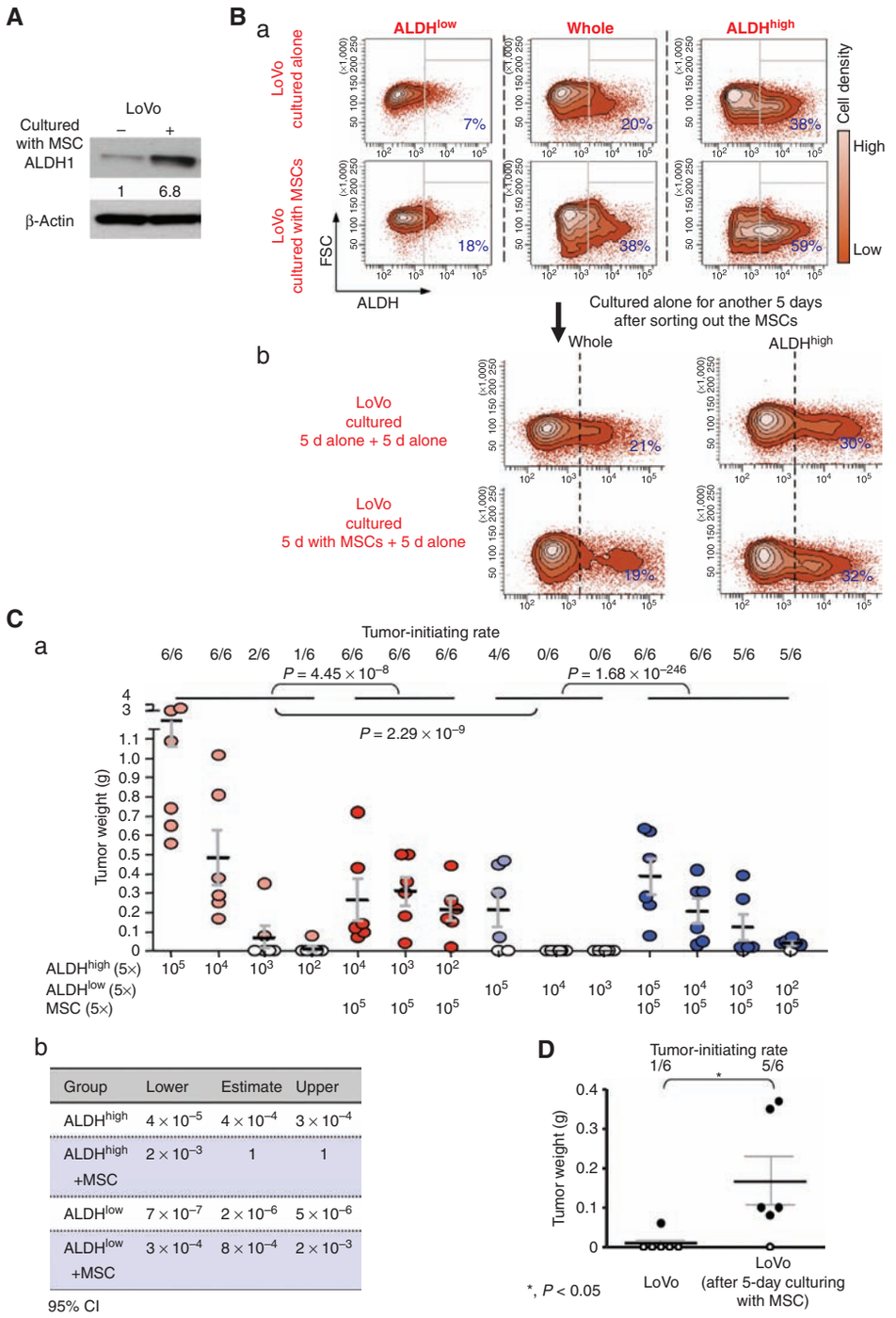

Figure 4. MSC-induced increase in tumor initiation is reflected in an increase in ALDH^{high} CSC-enriched populations. **A,** ALDH1 protein expression in LoVo cells cultured either alone or with MSCs. The numbers indicate relative protein levels. **B,** unsorted (whole) ALDH^{high} and ALDH^{low} LoVo cells were cultured either alone or with tdTomato-MSCs. After 5 days, ALDH activity of LoVo cells was analyzed by flow cytometry (a) and tdTomato-MSCs were removed from the cultures by flow sorting. After removing MSCs, the LoVo cells were cultured alone for another 5 days. The ALDH activities were again analyzed by flow cytometry (b). The percentages indicate the percentage of ALDH^{high} LoVo cells; that is, percent of LoVo cells with ALDH activity beyond the indicated thresholds. **C,** a, weights of tumors derived from ALDH^{high} or ALDH^{low} LoVo cells injected into SCID mice, either alone or with MSCs. Solid-filled and hash-filled circles indicate individual tumor weights; open circles indicate no tumor grew at the site of injection. Red circles: injection of ALDH^{high} LoVo cells. Blue circles: injection of ALDH^{low} LoVo cells. Hash-filled circles: injection of LoVo cells, solid-filled circles: injection of LoVo cells and MSCs. Bars are means ± SE. b, the ranges of the estimated tumor-initiating frequencies evaluated by ELDA. **D,** LoVo cells cultured with tdTomato-MSCs have increased numbers of TICs. Cells were cultured as in **B.** After isolating LoVo cells by sorting, cells (5×10^4 cells per injection) were injected into mice. After 6 weeks, the tumors were isolated and weighed. Filled circles indicate individual tumor weights. Open circles indicate no tumor grew at the site of injection. Bars are means ± SE.

alone (38%, 20%, and 7%), that is, 1.6- to 2.6-fold increases in ALDH^{high} cells (Fig. 4Ba).

We also used FACS analysis to remove the tdTomato-MSCs from LoVo/MSC cocultures, then further propagated the LoVo cells for 5 days in the absence of MSCs. We found that the levels of the ALDH^{high} LoVo cell subpopulations that had previously been increased by coculture with MSCs reverted to levels comparable with those observed in LoVo cells that had never experienced MSC coculture (Fig. 4Bb). Our data indicated that maintenance of elevated numbers of ALDH^{high} LoVo cells depended on continuous interactions of the LoVo cells with MSCs.

Use of the ALDH marker as the sole stem cell marker is likely to have led to an underestimate in the increase of the number of CSCs, as ALDH^{high} cells are a CSC-enriched population rather than being a pure CSC population. To refine the markers used to identify CSCs, we determined that a LoVo subpopulation more enriched for CSCs could be identified by concomitant use of the ALDH^{high} and CD133^{+} markers, which have been used to define CSCs in various cancer cell populations (refs. 22–25; described in Section 3, Supplementary Data; Supplementary Fig. S6A–C). Indeed, in the LoVo cells cocultured for 5 days with MSCs, the ALDH^{high}/CD133^{+} LoVo cells were increased from 1.4% to 16.4% of the overall cell population, that is, a 11.7-fold increase (Supplementary Fig. S6C).

We also determined whether the MSC-induced increase of ALDH^{high} LoVo cells observed in culture was accompanied by an increase of TICs in LoVo cells. Limiting dilutions of sorted ALDH^{high} and ALDH^{low} LoVo cells were injected subcutaneously into severe combined immunodeficient (SCID) mice, either alone or together with MSCs (Fig. 4Ca). As calculated using ELDA, the TIC frequency of ALDH^{high} LoVo cells injected on their own was 4×10^{-5} to 3×10^{-4}, whereas that of ALDH^{high} LoVo coinjected with MSCs was 2×10^{-3} to 1 (Fig. 4Cb). For ALDH^{low} LoVo cells injected alone, the TIC frequency was 7×10^{-7} to 5×10^{-6}; coinjection with MSCs increased this frequency to 3×10^{-4} to 2×10^{-3} (Fig. 4Cb). TIC frequencies of both ALDH^{high} and ALDH^{low} LoVo cells were increased by several orders of magnitude when coinjected with MSCs.

The continued presence of MSCs in the implanted cell populations complicates interpretation of the direct effects of MSC on the tumor initiation of carcinoma cells, as the MSCs might affect tumor initiation by a number of different mechanisms. To address this issue, LoVo cells or HCC1806 cells were isolated by FACS analysis from 5-day carcinoma cell/tdTomato-MSC cocultures and were then immediately injected subcutaneously into SCID mice, in parallel with LoVo cells previously cultured alone, to determine the effect on the tumor initiation of the cell culture interactions (Fig. 4D and Supplementary Fig. S7A). Accordingly, TIC frequencies of LoVo cells were increased by one order of magnitude following a 5-day coculture with MSCs *in vitro* (Supplementary Fig. S7B). An increase of tumor initiation by prior coculture with MSCs was also observed on HCC1806 cells (Supplementary Fig. S7C).

Influence of PGE_2 Signaling on the ALDH^{high} CSC State

To understand more precisely how the signals exchanged between carcinoma cells and MSCs led to increases in ALDH^{high} CSCs, we first ascertained whether PGE_2 and/or cytokines produced by MSCs in LoVo/MSC cocultures could elicit ALDH1 expression. Only PGE_2 was able, on its own, to elicit an increase in ALDH1 expression in LoVo cells (Fig. 5A). Moreover, when PGE_2 was combined with the 4 cytokines, there was no further increase in ALDH1 expression.

EP4 is the only PGE_2 receptor highly expressed by LoVo cells (Supplementary Fig. S2G). To elucidate in more depth the effects of PGE_2 on LoVo cells, we treated these cells with vehicle or PGE_2 for 5 days. The vehicle-treated cultures contained 10.3% ALDH^{high} LoVo cells, whereas the LoVo cells treated with PGE_2 contained approximately 25% ALDH^{high} LoVo cells (Fig. 5B). We added GW627368X (the EP4 receptor antagonist) to LoVo cells to determine whether the basal, unperturbed levels of ALDH^{high} cells depended on ongoing PGE_2 autocrine signaling; this treatment reduced by approximately 60% the basal level of ALDH^{high} LoVo cells (Fig. 5B). These data suggested that within LoVo cells, subpopulations of cells are maintained in an ALDH^{high} state, in part, through ongoing, low-level autocrine PGE_2 signaling. Moreover, this signaling and associated entrance into the ALDH^{high} state could be enhanced by exogenously supplied PGE_2.

The observed increase in ALDH1 expression induced by PGE_2 was not confined to LoVo cells. PGE_2 treatment induced elevated ALDH1 expression (2.9- to 12.9-fold) in LoVo, SUM149, SUM159, and BT549 cells (Fig. 5C), all of which were previously found to elicit increased PGE_2 production from cocultured MSCs.

The LoVo cells that had been treated *ex vivo* with vehicle or PGE_2 for 5 days were implanted subcutaneously in SCID mice. Tumors derived from control LoVo cells occurred in 3 of 16 injected hosts, whereas the corresponding PGE_2-treated cells formed tumors in 18 of 24 hosts (Fig. 5D). Hence, a substantial increase in ALDH^{high} cells and TICs could be achieved by PGE_2 treatment of LoVo cells *ex vivo*. Moreover, treating LoVo cells with the cocktail of cytokines (IL-6, IL-8, GRO-α, and RANTES) in addition to PGE_2 did not significantly increase the tumor initiation beyond that observed for PGE_2 treatment alone (Supplementary Fig. S8). In addition to its effects on TICs, PGE_2 is likely to contribute to the maintenance of CSCs *in vivo* by increasing tumor angiogenesis (Supplementary Fig. S9, discussed in Supplementary Data, section 4).

Role of PGE_2 Signaling in the MSC-Induced ALDH^{high} CSC-Enriched Population and Tumor Initiation

To confirm that the above-described role of PGE_2 could explain the ability of MSCs to induce CSC formation, we inhibited PGE_2 synthesis with NS398, or PGE_2 signaling with GW627368X, in cocultures of LoVo cells and tdTomato-MSCs. Blocking PGE_2 signaling by either route prevented most of the increases in ALDH^{high} LoVo CSCs by MSCs (described in Section 5, Supplementary Data; Supplementary Fig. S10). LoVo cells that had been cocultured under the various conditions with MSCs for 5 days were sorted by FACS analysis to eliminate tdTomato-MSCs and were then injected subcutaneously into SCID mice. The increase in TIC frequencies resulting from a 5-day coculture with MSCs (from 4/20 to 14/19) was prevented by introducing either NS398 or GW627368X into the cocultures (from 14/19 to 3/17 or

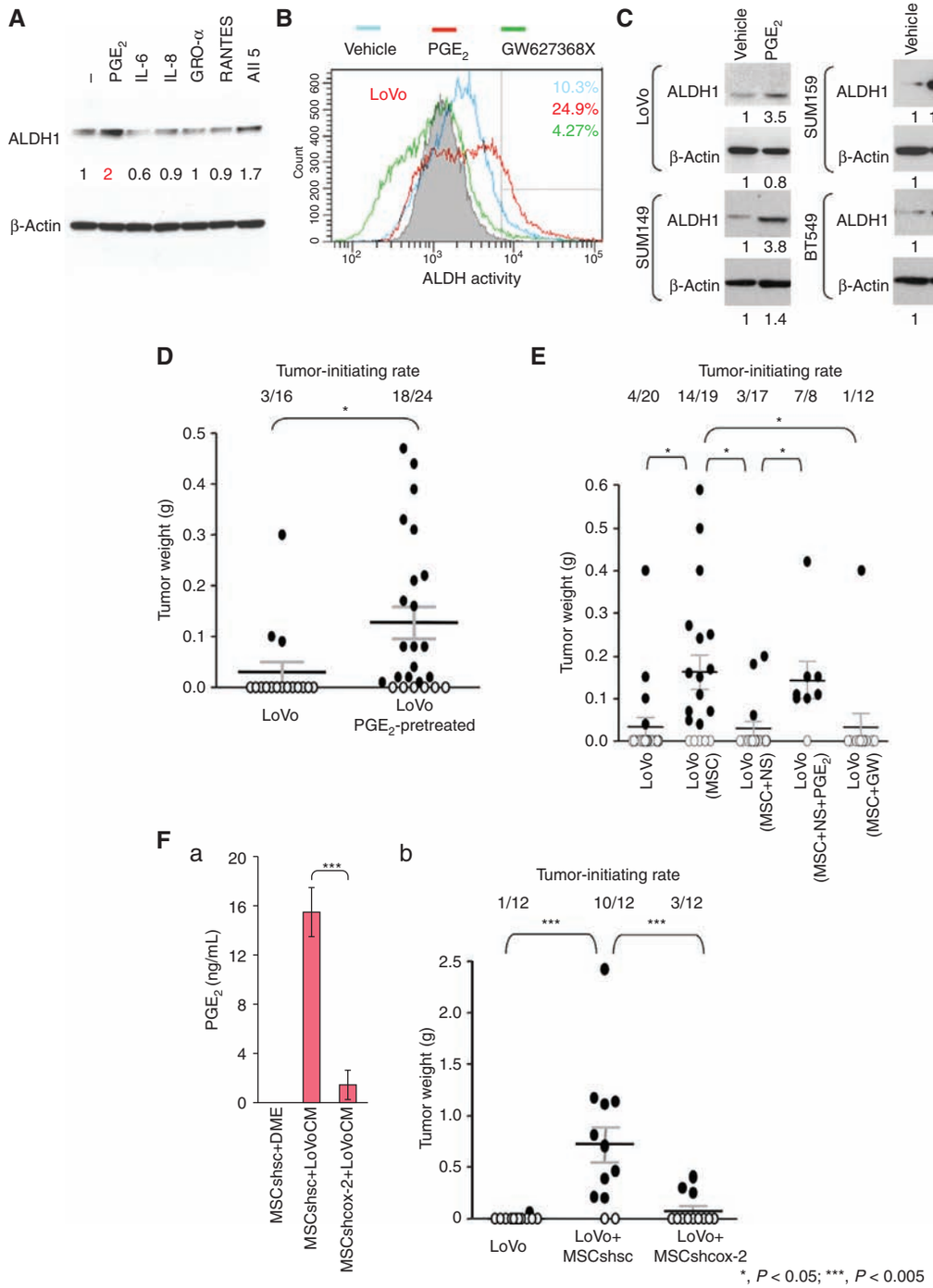

Figure 5. COX-2-PGE$_2$ signaling is required for MSC-induced increase in ALDH^{high} CSC-enriched population and tumor initiation. **A,** ALDH1 protein expression in LoVo cells treated as indicated for 5 days. **B,** ALDH activity of LoVo cells treated with vehicle, PGE$_2$ (100 nmol/L), or GW627368X (20 μmol/L) was analyzed by flow cytometry. The percentages indicate the percentage of ALDH^{high} LoVo cells; that is, LoVo cells with ALDH activity beyond the indicated thresholds. The gray line at the right side of the plot indicates the threshold of the high ALDH activity. **C,** ALDH1 protein levels in various carcinoma cells treated with vehicle or PGE$_2$. The numbers indicate relative protein levels. **D,** PGE$_2$ increases LoVo TICs. LoVo cells pretreated with vehicle or PGE$_2$ (100 nmol/L) were injected into SCID mice (5×10^4 cells per injection). After 6 weeks, tumors were isolated and weighed. Bars are means ± SE. **E,** LoVo cells were cultured with tdTomato-MSCs, PGE$_2$, NS398, or GW627368X, as indicated. After 5 days, the LoVo cells were isolated by cell sorting and injected into SCID mice (5×10^4 cells per injection). After 7 weeks, the tumors were isolated and weighed. Filled circles indicate individual tumor weights; open circles indicate no tumor grew at the site of injection. Bars are means ± SE. **F,** a, levels of PGE$_2$ secreted by LoVoCM-treated MSCshsc and MSCshcox-2. Data are means ± SE, $n = 3$. b, weights of tumors derived from LoVo cells (5×10^4 cells per injection) injected into SCID mice either alone, with MSCshsc, or with MSCshcox-2 (2×10^5 cells per injection). Filled circles indicate individual tumor weights; open circles indicate no tumor grew at the site of injection. Bars are means ± SE.

1/12, respectively, Fig. 5E). Adding PGE_2 to the cocultures along with NS398 restored the tumor-initiating frequency from 3/17 to 7/8.

To validate the role of COX-2 in these properties, we knocked down COX-2 in MSCs. The ability of the resulting MSCshcox-2 cells to produce PGE_2 in response to LoVoCM was reduced by 90% (Fig. 5Fa). The tumor-initiating frequency of 5×10^4 LoVo cells was increased from 1/12 to 10/12 by coinjection with MSCs expressing a control, scrambled shRNA (MSCshsc cells; Fig. 5Fb). In contrast, in mice coinjected with MSCshcox-2 cells, the tumor-initiating frequency of LoVo cells was increased from 1/12 to only 3/12, supporting the notion that COX-2-dependent PGE_2 induced in MSCs was required for the observed robust increases of LoVo TICs.

PGE_2 Induces β-Catenin Nuclear Localization and Transactivation

The β-catenin signaling pathway has been implicated in maintaining stem cell and CSC homeostasis in most epithelial tissues (26, 27). Relevant here is the finding that PGE_2 treatment leads to Akt activation; activated Akt subsequently stimulates β-catenin signaling in several ways (28, 29). Accordingly, we examined activation of Akt/glycogen synthase kinase-3 (GSK-3)/β-catenin signaling axis in LoVo cells treated with vehicle, PGE_2, GW627368X, or GW627368X + PGE_2. We found that PGE_2 treatment led to a 12-fold increase in Akt phosphorylation at Thr473 (Fig. 6A), which indicates functional Akt activation (30). Conversely, inhibiting PGE_2 signaling with GW627368X in PGE_2-treated LoVo cells blocked 50% of the PGE_2-induced Akt phosphorylation (Fig. 6A). Moreover, β-catenin activity is positively affected by Akt-mediated phosphorylation of its Ser552 residue (31, 32). PGE_2 treatment of LoVo cells, which caused a 12-fold increase of Akt phosphorylation, also increased β-catenin phosphorylation at Ser552 (11-fold), an increase that was blocked entirely by GW627368X treatment (Fig. 6A).

Akt also enhances β-catenin by phosphorylating and thereby inactivating GSK-3; this prevents inactivation of β-catenin by unphosphorylated GSK-3, as Ser21-unphosphorylated GSK-3α and Ser9-unphosphorylated GSK-3β phosphorylate β-catenin at its Ser33/Ser37/Thr41 residues, leading to its degradation (33, 34). PGE_2 strongly increased the phosphorylation of GSK-3α at Ser21 (56-fold above basal level, Fig. 6A). Although Ser9 of GSK-3 was already phosphorylated before PGE_2 treatment, this basal level of GSK-3β Ser9 phosphorylation was reduced (70%) by adding GW627368X (Fig. 6A), presumably by blocking basal autocrine PGE_2 signaling. Inhibition of PGE_2 signaling by GW627368X prevented the inactivating phosphorylation of GSK-3α and GSK-3β and, conversely, increased phosphorylation of β-catenin at Ser33/Ser37/Thr41 residues that lead to its degradation by 15-fold (Fig. 6A). These data indicated that inhibition of PGE_2 signaling leads to β-catenin phosphorylation, a prelude to its proteasomal degradation.

A strong inhibition of β-catenin signaling is also achieved by E-cadherin, which recruits β-catenin to adherens junctions associated with the plasma membrane, thereby preventing its nuclear localization and its actions in promoting transcription (35). PGE_2 decreased the E-cadherin and ZO-1 protein located at the cell junctions (Fig. 6B and C). Correspondingly, in PGE_2-treated LoVo cells, β-catenin was found in cell nuclei, rather than being sequestered by E-cadherin in adherens junctions (Fig. 6B and C). PGE_2 caused a 5.3-fold increase of β-catenin in the nuclear fraction; this increase was blocked by adding the EP4 antagonist during PGE_2 treatment (Fig. 6D). We also found, by analyzing expression in LoVo carcinoma cells of a number of β-catenin/TCF-regulated genes, that PGE_2-induced nuclear β-catenin was functionally active (Fig. 6E).

PGE_2-Induced Effects on $ALDH^{high}$ Cancer Cells Are Mediated by β-Catenin Signaling

PGE_2 induces Akt phosphorylation in carcinoma cells in a phosphatidylinositol 3-kinase (PI3K)-dependent manner (28). To determine whether the activation of the Akt/GSK-3/β-catenin signaling axis was required for PGE_2-induced $ALDH^{high}$ LoVo CSCs, we treated $ALDH^{high}$ LoVo cells with vehicle, PGE_2, GW627368X, LY294002 (a PI3K inhibitor), FH353 (a β-catenin/TCF inhibitor), or cardamonin (a β-catenin inhibitor) for 5 days at concentrations that did not cause significant cell death.

LY294002 functioned as efficiently as the EP4 antagonist by completely blocking the exogenous PGE_2-induced increase of $ALDH^{high}$ LoVo cells and by decreasing the endogenous PGE_2-maintained basal $ALDH^{high}$ LoVo cells (Fig. 6F, a and d). Although the 2 β-catenin inhibitors FH353 and cardamonin blocked the PGE_2-induced increase of $ALDH^{high}$ LoVo cells (Fig. 6Fb and Fc), these inhibitors did not function as effectively as the EP4 antagonist or the PI3K inhibitor. PGE_2/EP4 signaling, acting through the Akt/GSK-3/β-catenin signaling axis (28), contributes to induction of the $ALDH^{high}$ LoVo cell phenotype.

Contribution of MSCs in Tumor Stroma to the Stem Cell Niche of $ALDH^{high}$ CSCs

PGE_2 is metabolically unstable and is thought to act within tissues over short distances, doing so in both an autocrine and a paracrine manner. Wishing to pursue this notion further, we examined whether $ALDH^{high}$ CSCs were located near MSCs (or their mesenchymal derivatives) in tumors that arose following the coinjection of these 2 cell types. $ALDH^{high}$ LoVo cells (Fig. 7Aa, red signal) were often surrounded by tdTomato-labeled MSCs (Fig. 7Aa, green signal) or their derivatives in tissue sections of LoVo/MSC xenografts; in addition, many of these mesenchymal cells expressed COX-2 (Fig. 7Aa, cyan signal). Moreover, the mesenchymal cells associated with the $ALDH^{high}$ tumor cells expressed FSP, the fibroblast marker (Fig 7Ab, red signal; discussed in Supplementary Data, section 6; Supplementary Fig. S11), indicating that the MSC-derived fibroblasts rather than their MSC precursors were largely responsible for forming the stromal microenvironment of these $ALDH^{high}$ cells. The conclusion that PGE_2 induces the formation of $ALDH^{high}$ CSCs was further supported by human colorectal adenocarcinoma studies in which we found the juxtaposition within tumors of such CSCs with stroma expressing COX-2, the likely source of PGE_2 production (discussed in Supplementary Data, section 7; Supplementary Fig. S12A and B). These observations lead us to propose that MSCs (or their differentiated derivatives) create a niche within tumors, leading to induction and/or maintenance of CSC subpopulations.

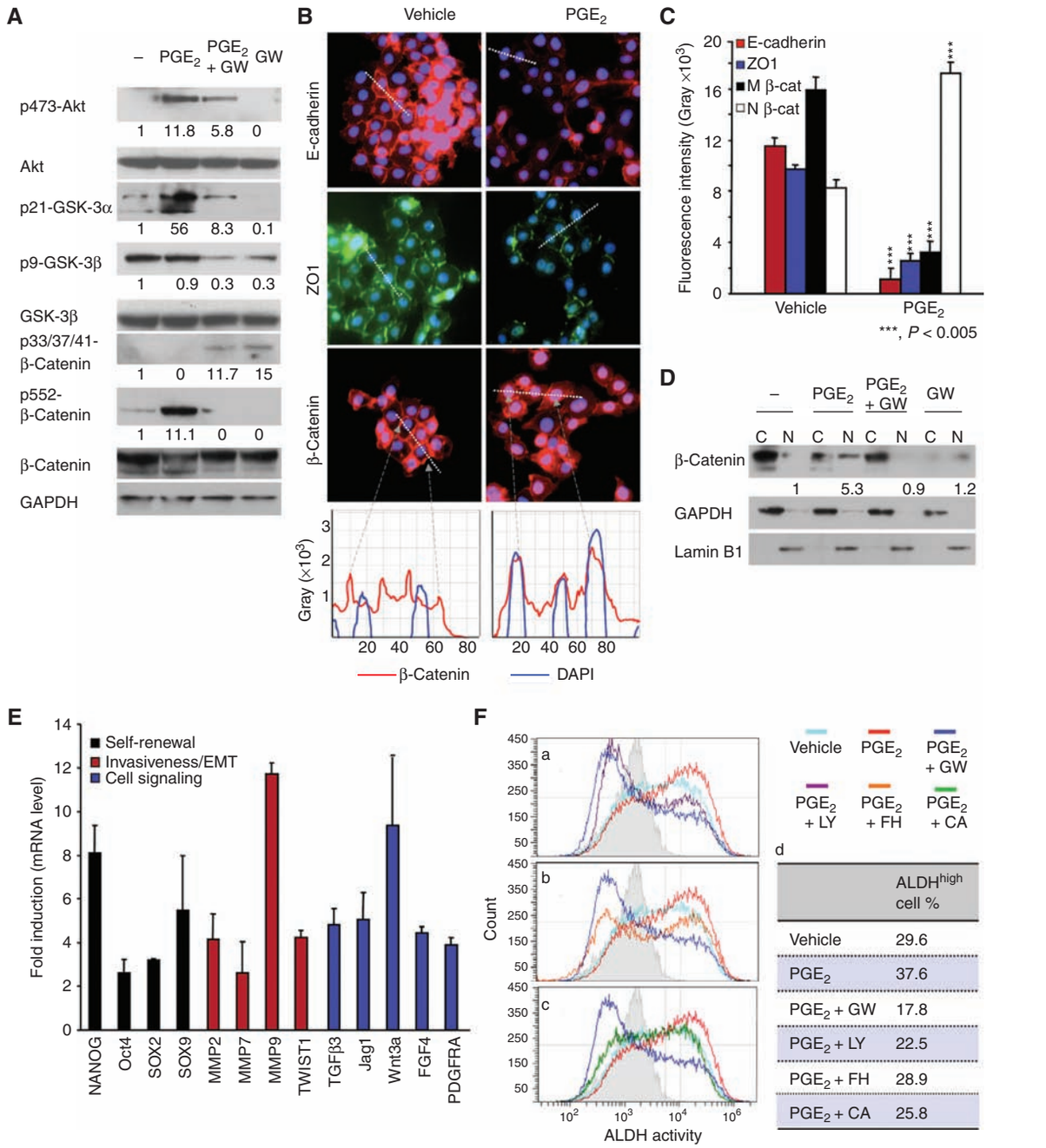

Figure 6. PGE$_2$ induces ALDH^{high} cancer cells through the Akt/GSK-3/β-catenin signaling axis. **A,** activation of Akt/GSK-3/β-catenin signaling in LoVo cells treated as indicated for 1 hour was analyzed by Western blots for phosphorylated Akt, total Akt, phosphorylated GSK-3α, phosphorylated GSK-3β, total GSK-3β, phosphorylated β-catenin, total β-catenin, and glyceraldehyde-3-phosphate dehydrogenase (GAPDH). The numbers indicate relative protein levels. **B,** the distribution of E-cadherin (red), ZO-1 (green), and β-catenin (red) in LoVo cells treated with vehicle or PGE$_2$ (100 nmol/L) for 48 hours was analyzed by immunofluorescence. Cell nuclei were stained with DAPI (4′6-diamidino-2-phenylindole, in blue). The graphs show the fluorescence intensities along the dashed lines in the images of β-catenin staining. β-Catenin intensities are in red lines and DAPI intensities are in blue lines. **C,** quantification of the levels of E-cadherin, ZO-1, and β-catenin associated with membrane and of nuclear β-catenin. The fluorescence intensities for the staining of these proteins in randomly selected cells in images (e.g., the cells crossed by dashed lines in (**B**) were quantified. Bars are means ± SE, $n > 50$ for each bar. M β-cat, membrane-bound β-catenin; N β-cat, nuclear β-catenin. **D,** nuclear/cytosolic distribution of β-catenin in LoVo cells treated as indicated was analyzed by Western blot of β-catenin, GAPDH, and lamin B1, a nuclear envelope marker, in nuclear and cytosolic fractions. **E,** mRNA expression of selected β-catenin/TCF-dependent genes in LoVo cells treated with vehicle or PGE$_2$ for 7 hours. The mRNA levels of these genes were normalized to GAPDH mRNA. Data are fold induction by PGE$_2$ (vs. that of vehicle-treated LoVo cells). Data are means ± SE, $n = 3$. **F,** ALDH activities of ALDH^{high} LoVo cells treated with vehicle, PGE$_2$, PGE$_2$ + GW627368X (GW; 20 μmol/L), PGE$_2$ + LY294002 (0.5 μmol/L), or PGE$_2$ + FH535 (6 μmol/L) for 5 days (a–c). Percentages of ALDH^{high} LoVo cells are presented in the table (d). The gray lines at the right side of the plots indicate the thresholds of the high ALDH activity.

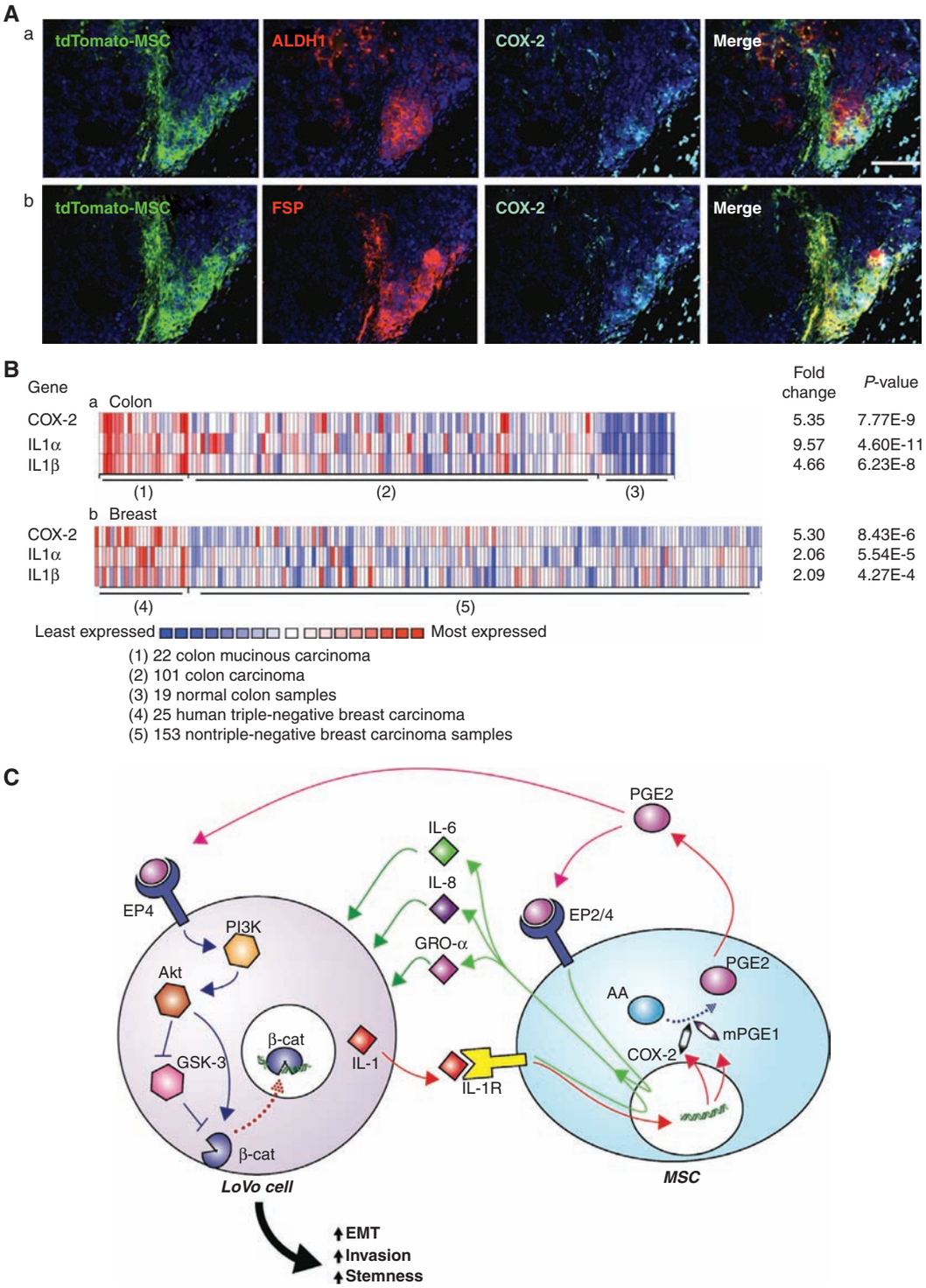

Figure 7. MSCs in tumor stroma serve as an ALDH^{high} cancer stem cell niche. **A,** immunofluorescence analyses were carried out on tumors derived from LoVo cells (5×10^4 cells per injection) injected along with tdTomato-MSCs (5×10^5 cells per injection), using antibodies against tdTomato-RFP (in green), ALDH1 (in red, panel a), fibroblast surface protein FSP (in red, panel b), and COX-2 (cyan). Panels a and b are serial sections from one tumor. Scale bar, 100 μm. **B,** IL-1 and COX-2 mRNA expression in human colon and breast carcinoma. The "fold change" indicates the average mRNA levels of the 3 genes in colon mucinous carcinoma samples, compared with that of normal colon samples (panel a) and in TNBC samples, compared with that of non-TNBC samples (panel b). **C,** the proposed interactions for induction and maintenance of EMT, cancer cell stemness, and invasiveness by MSCs. AA, arachidonic acid.

Correlation of COX-2 Expression with CSC Properties and a More Aggressive Tumor Phenotype

To determine whether elevated IL-1 production correlates with COX-2/PGE_2 expression in human primary carcinomas, we compared the normalized IL-1α, IL-1β, and COX-2 mRNA levels across 19 human normal colon and 123 human colon carcinoma samples and across 178 human invasive breast carcinoma samples (Cancer Genome Atlas analyzed by Oncomine). IL-1α and IL-1β were expressed at significantly higher levels (9.6-fold and 4.7-fold in colon carcinoma and 2.1-fold and 2.1-fold in breast carcinoma) in aggressive subtypes of samples—colon mucinous carcinoma and triple-negative breast carcinoma (TNBC), respectively (Fig. 7B). Moreover, the COX-2 mRNA levels were correlated with the IL-1α and IL-1β mRNA levels; COX-2 mRNA was elevated 5.4-fold and 5.3-fold in colon mucinous carcinoma and TNBC when compared with normal colon samples and other breast cancers (Fig. 7B). These correlations suggested that the signaling mechanisms described above (Fig. 7C), involving IL-1–activated expression of COX-2/PGE_2, may be relevant to understanding the pathogenesis of colon mucinous carcinomas and TNBCs.

DISCUSSION

Elevated IL-1 expression has been correlated with increased malignant progression and more aggressive phenotypes in many types of cancer (36). However, the mechanism(s) underlying this correlation have been unclear. We describe here a bidirectional, reciprocal interaction between carcinoma cells and the MSCs (Fig. 7C). The signaling is initiated through the release of IL-1 by carcinoma cells. We present evidence that seems to explain this connection between IL-1 production and increased tumor aggressiveness in many, and perhaps all, IL-1–secreting carcinomas.

IL-1 secreted by carcinoma cells induces COX-2 and mPGES1 expression in MSCs. The 2 enzymes collaborate in MSCs to generate PGE_2 levels, which can increase by 80- to 500-fold (Fig. 1Cb). Of note, we show these responses operate equally well in MSCs and in their more differentiated descendants (Supplementary Fig. S2D and S2E). We note that others recently reported that IL-1 secreted by head and neck squamous cell carcinoma cells induce PGE_2 from fibroblasts (37). Consequently, fibroblasts and myofibroblasts, both of which accumulate in large numbers in the stroma, may also represent sources of the PGE_2 and the subsequently produced cytokines described here.

Importantly, although COX-2 is highly expressed in both neoplastic and stromal cells in tumors, not all COX-2-expressing cells can produce PGE_2. Thus, despite large variations in COX-2 expression, the colorectal carcinoma cell lines that we examined produced only about 10 to 40 pg/mL of PGE_2 (Supplementary Fig. S1A). These levels are dwarfed by the 15,000 to 40,000 pg/mL of PGE_2 produced by the IL-1–stimulated MSCs studied here (Fig. 1Cb). This failure by COX-2-expressing carcinoma cells to produce significant levels of PGE_2 may be due to the absence in many carcinoma cells of significant levels of mPGES1 expression (Supplementary Fig. S1A and S1D). Hence, COX-2 expression, on its own, is unlikely to provide an accurate indication of PGE_2 production by carcinomas.

MSC-produced PGE_2 acts in 2 ways within such tumors—in an autocrine fashion on the MSCs that produced it and in a paracrine fashion on the nearby IL-1–releasing carcinoma cells. The MSC autocrine signaling elicits a second wave of signaling responses: In collaboration with ongoing paracrine IL-1 signaling from carcinoma cells, the autocrine PGE_2 induces IL-6, IL-8, GRO-α, and RANTES cytokines in the MSCs. Together, these MSC-derived molecules induce a third wave of responses that profoundly alter the carcinoma cells that initiated this signaling cascade (Fig. 2E and 7C).

The changes induced in carcinoma cells by the confluence of PGE_2 and cytokine signals are all components of the complex cell–biological program termed EMT. Although this program has been increasingly implicated in the acquisition of phenotypes associated with high-grade malignancy (14), major questions concerning EMT have remained unanswered. Among them are the paracrine signals, ostensibly of stromal origin, that trigger EMT in carcinoma cells. Here we present a scenario that explains how EMT can be induced in carcinoma cells by a reactive stroma.

This work also addresses another longstanding puzzle about EMT: Is it usually activated as a single, coherent program or, alternatively, are distinct components of this program activated separately, each by a distinct set of heterotypic signals? Our observations indicate that the latter scenario is more likely. For example, PGE_2 caused a decrease of E-cadherin expression in carcinoma cells, whereas cytokines were required to induce the vimentin and ZEB1 expression that is usually depicted as intrinsic components of the EMT program (Fig. 3B). Such responses suggest the possibility that, during the course of spontaneous tumor progression, some carcinoma cells may receive only a subset of these signals and accordingly only activate portions of the EMT program, whereas the others receiving the complete suite of heterotypic signaling molecules may pass through an entire EMT program.

Research by ourselves and others has connected EMT with entrance into a stem cell–like state, both in normal and neoplastic epithelial cells (12, 13, 17). These findings are also echoed by this work, in which we observed a concomitant entrance into the mesenchymal and stem cell states in response to MSC-derived heterotypic signals. PGE_2, which activated portions of the EMT program, was able to increase both the number of CSCs and the frequency of tumor initiation (Fig. 5A–D). Our findings here further clarify the connection of EMT with entrance into a stem cell–like state by showing that the partial EMT induced by PGE_2, which represses cell–cell junctions without inducing mesenchymal traits, suffices to increase CSCs. The observation of MSC-induced increases in CSCs is consistent with the recent finding of prostaglandin-induced increases in the number of $CD44^+$ tumor cells (38, 39). The unique contribution of PGE_2 is underscored by the observation that other MSC-derived cytokines, when combined with PGE_2, had only marginal effects on further increasing the TIC frequency (Supplementary Fig. S8).

In earlier work (27), we documented an alternative means of activating the EMT program that involves canonical and noncanonical WNTs, together with TGFβ. Those findings echoed the present observations, as both studies showed that multiple

distinct heterotypic signals, acting in concert, are required to activate an EMT in carcinoma cells. These earlier findings left open the possibility that other EMT-inducing signals beyond those documented at the time may converge on the WNT and TGF-β signaling pathways to activate EMT programs. We note here that PGE_2-activated signals do, indeed, converge on one of these signaling cascades by activating β-catenin signaling, the same pathway that represents the main signaling channel lying downstream of canonical WNT signaling.

In tumors that arise from IL-1–producing carcinoma cells, we find that this interleukin plays a critical role in the tumor cell–induced COX-2/mPGES1/PGDH/PGE_2 response in MSCs that is required for tumor progression. IL-1 blockage has been used in thousands of patients to control infection and inflammatory disease and has a remarkable safety record (40). On the basis of our findings and the existing clinical use of IL-1 inhibitors, IL-1 inhibition may present a promising alternative to COX-2 inhibitors for cancer therapy. In addition, limited therapeutic options are currently available for TNBCs, which produce higher levels of IL-1 (Fig. 7B), because they are unresponsive to standard receptor–mediated treatments. Accordingly, our findings suggest a possible option for treating these aggressive subtypes of breast and colon cancer.

METHODS

Cell Culture

Human carcinoma cell lines HCC1806, BT549, MDA-MB-231, MDA-MB-453, SW1116, and LoVo were obtained from American Type Culture Collection and human bone marrow–derived MSCs (Sciencell) were obtained from Sciencell. SUM149 and SUM159 cells were provided by S.P. Ethier (Wayne State University, Detroit, MI). The human carcinoma cell lines SUM149, SUM159, BT549, MDA-MB-231, MDA-MB-453, SW1116, and LoVo were authenticated by microarray analysis. HCC1806 and MSC were not passaged more than 6 months after receipt.

Animal Experiments

All research involving animals complied with protocols approved by the MIT Committee on Animal Care. In experiments evaluating tumor initiation and growth, the tumors were isolated and weighed at the end of each experiment. To measure TIC frequency, serial dilutions of cancer cell suspensions were injected subcutaneously into nude mice. TIC frequencies of the samples were determined using the ELDA webtool (18).

PGE_2 and Cytokine Assays

The concentrations of PGE_2 and cytokines were determined by ELISA as described in the manufacturers' protocols. PGE_2 levels were measured using a PGE_2 direct Biotrack assay kit (GE Healthcare). Human cytokine levels were measured using Quantikine kits (R&D Systems).

Invasion Assay

Cell invasion was evaluated by using BD Matrigel Invasion Chambers, 8.0 μm (BD Biosciences). The cells that migrated through the membrane during the incubation period were counted in 5 randomly selected regions.

See Supplementary Materials and Methods for more information.

Disclosure of Potential Conflicts of Interest

No potential conflicts of interest were disclosed.

Authors' Contributions

Conception and design: H.-J. Li, H.R. Herschman, R.A. Weinberg
Development of methodology: H.-J. Li, H.R. Herschman
Acquisition of data (provided animals, acquired and managed patients, provided facilities, etc.): H.-J. Li, F. Reinhardt
Analysis and interpretation of data (e.g., statistical analysis, biostatistics, computational analysis): H.-J. Li, H.R. Herschman
Writing, review, and/or revision of the manuscript: H.-J. Li, H.R. Herschman, R.A. Weinberg
Administrative, technical, or material support (i.e., reporting or organizing data, constructing databases): H.-J. Li, H.R. Herschman
Study supervision: H.R. Herschman, R.A. Weinberg

Acknowledgments

The authors thank members of the Weinberg laboratory (Wai Leong Tam, Michael Hwang) and the Herschman laboratory (Tomo-o Ishikawa, Art Catapang) for discussion and technical support; the Whitehead Flow Cytometry Core for technical support; and Sarah Dry and the UCLA Translational Pathology Core Laboratory for providing colon adenocarcinoma samples.

Grant Support

The work was supported by Breast Cancer Research Foundation (R.A. Weinberg), Susan G. Komen for the Cure (H.-J. Li), NIH (R.A. Weinberg: U54CA163109 and H.R. Herschman: R01CA123055 and P50CA086306), and Ludwig Center for Molecular Oncology (R.A. Weinberg).

Received March 9, 2012; revised June 21, 2012; accepted June 22, 2012; published OnlineFirst July 3, 2012.

REFERENCES

1. Bhowmick NA, Moses HL. Tumor-stroma interactions. Curr Opin Genet Dev 2005;15:97–101.
2. Salem HK, Thiemermann C. Mesenchymal stromal cells: current understanding and clinical status. Stem Cells 2010;28:585–96.
3. Karnoub AE, Dash AB, Vo AP, Sullivan A, Brooks MW, Bell GW, et al. Mesenchymal stem cells within tumour stroma promote breast cancer metastasis. Nature 2007;449:557–63.
4. Mishra PJ, Humeniuk R, Medina DJ, Alexe G, Mesirov JP, Ganesan S, et al. Carcinoma-associated fibroblast-like differentiation of human mesenchymal stem cells. Cancer Res 2008;68:4331–9.
5. Quante M, Tu SP, Tomita H, Gonda T, Wang SS, Takashi S, et al. Bone marrow-derived myofibroblasts contribute to the mesenchymal stem cell niche and promote tumor growth. Cancer Cell 2011;19:257–72.
6. Liu S, Ginestier C, Ou SJ, Clouthier SG, Patel SH, Monville F, et al. Breast cancer stem cells are regulated by mesenchymal stem cells through cytokine networks. Cancer Res 2011;71:614–24.
7. Menter DG, Schilsky RL, DuBois RN. Cyclooxygenase-2 and cancer treatment: understanding the risk should be worth the reward. Clin Cancer Res 2010;16:1384–90.
8. Wang D, Dubois RN. Eicosanoids and cancer. Nat Rev Cancer 2010; 10:181–93.
9. Ishikawa TO, Herschman HR. Tumor formation in a mouse model of colitis-associated colon cancer does not require COX-1 or COX-2 expression. Carcinogenesis 2010;31:729–36.
10. Le Bitoux MA, Stamenkovic I. Tumor-host interactions: the role of inflammation. Histochem Cell Biol 2008;130:1079–90.
11. Bomken S, Fiser K, Heidenreich O, Vormoor J. Understanding the cancer stem cell. Br J Cancer 2010;103:439–45.
12. Mani SA, Guo W, Liao MJ, Eaton EN, Ayyanan A, Zhou AY, et al. The epithelial-mesenchymal transition generates cells with properties of stem cells. Cell 2008;133:704–15.
13. Guo W, Keckesova Z, Donaher JL, Shibue T, Tischler V, Reinhardt F, et al. Slug and Sox9 cooperatively determine the mammary stem cell state. Cell 2012;148:1015–28.

14. Thiery JP, Acloque H, Huang RY, Nieto MA. Epithelial-mesenchymal transitions in development and disease. Cell 2009;139:871–90.
15. Tipton DA, Flynn JC, Stein SH, Dabbous M. Cyclooxygenase-2 inhibitors decrease interleukin-1beta-stimulated prostaglandin E2 and IL-6 production by human gingival fibroblasts. J Periodontol 2003;74:1754–63.
16. Houghton J, Stoicov C, Nomura S, Rogers AB, Carlson J, Li H, et al. Gastric cancer originating from bone marrow-derived cells. Science 2004;306:1568–71.
17. Morel AP, Lievre M, Thomas C, Hinkal G, Ansieau S, Puisieux A. Generation of breast cancer stem cells through epithelial-mesenchymal transition. PLoS One 2008;3:e2888.
18. Hu Y, Smyth GK. ELDA: extreme limiting dilution analysis for comparing depleted and enriched populations in stem cell and other assays. J Immunol Methods 2009;347:70–8.
19. Visvader JE. Cells of origin in cancer. Nature 2011;469:314–22.
20. Douville J, Beaulieu R, Balicki D. ALDH1 as a functional marker of cancer stem and progenitor cells. Stem Cells Dev 2009;18:17–25.
21. Huang EH, Hynes MJ, Zhang T, Ginestier C, Dontu G, Appelman H, et al. Aldehyde dehydrogenase 1 is a marker for normal and malignant human colonic stem cells (SC) and tracks SC overpopulation during colon tumorigenesis. Cancer Res 2009;69:3382–9.
22. Ma S, Chan KW, Lee TK, Tang KH, Wo JY, Zheng BJ, et al. Aldehyde dehydrogenase discriminates the CD133 liver cancer stem cell populations. Mol Cancer Res 2008;6:1146–53.
23. Silva IA, Bai S, McLean K, Yang K, Griffith K, Thomas D, et al. Aldehyde dehydrogenase in combination with CD133 defines angiogenic ovarian cancer stem cells that portend poor patient survival. Cancer Res 2011;71:3991–4001.
24. Lin L, Liu Y, Li H, Li PK, Fuchs J, Shibata H, et al. Targeting colon cancer stem cells using a new curcumin analogue, GO-Y030. British J Cancer 2011;105:212–20.
25. Kryczek I, Liu S, Roh M, Vatan L, Szeliga W, Wei S, et al. Expression of aldehyde dehydrogenase and CD133 defines ovarian cancer stem cells. Int J Cancer J Int du Cancer 2012;130:29–39.
26. Reya T, Clevers H. Wnt signalling in stem cells and cancer. Nature 2005;434:843–50.
27. Scheel C, Eaton EN, Li SH, Chaffer CL, Reinhardt F, Kah KJ, et al. Paracrine and autocrine signals induce and maintain mesenchymal and stem cell States in the breast. Cell 2011;145:926–40.
28. Castellone MD, Teramoto H, Williams BO, Druey KM, Gutkind JS. Prostaglandin E2 promotes colon cancer cell growth through a Gs-axin-beta-catenin signaling axis. Science 2005;310:1504–10.
29. Dorsam RT, Gutkind JS. G-protein-coupled receptors and cancer. Nat Rev Cancer 2007;7:79–94.
30. Fayard E, Xue G, Parcellier A, Bozulic L, Hemmings BA. Protein kinase B (PKB/Akt), a key mediator of the PI3K signaling pathway. Curr Top Microbiol Immunol 2010;346:31–56.
31. He XC, Yin T, Grindley JC, Tian Q, Sato T, Tao WA, et al. PTEN-deficient intestinal stem cells initiate intestinal polyposis. Nat Genet 2007;39:189–98.
32. Sun J. Enteric bacteria and cancer stem cells. Cancers (Basel) 2011; 3:285–97.
33. Haq S, Michael A, Andreucci M, Bhattacharya K, Dotto P, Walters B, et al. Stabilization of beta-catenin by a Wnt-independent mechanism regulates cardiomyocyte growth. Proc Natl Acad Sci U S A 2003; 100:4610–5.
34. Fukumoto S, Hsieh CM, Maemura K, Layne MD, Yet SF, Lee KH, et al. Akt participation in the Wnt signaling pathway through Dishevelled. J Biol Chem 2001;276:17479–83.
35. Orsulic S, Huber O, Aberle H, Arnold S, Kemler R. E-cadherin binding prevents beta-catenin nuclear localization and beta-catenin/LEF-1-mediated transactivation. J Cell Sci 1999;112:1237–45.
36. Miller LJ, Kurtzman SH, Anderson K, Wang Y, Stankus M, Renna M, et al. Interleukin-1 family expression in human breast cancer: interleukin-1 receptor antagonist. Cancer Invest 2000;18:293–302.
37. Alcolea S, Anton R, Camacho M, Soler M, Alfranca A, Aviles-Jurado FX, et al. Interaction between head and neck squamous cell carcinoma cells and fibroblasts in the biosynthesis of PGE2. J Lipid Res 2012;53:630–42.
38. Rudnick JA, Arendt LM, Klebba I, Hinds JW, Iyer V, Gupta PB, et al. Functional heterogeneity of breast fibroblasts is defined by a prostaglandin secretory phenotype that promotes expansion of cancer-stem like cells. PLoS One 2011;6:e24605.
39. Ishimoto T, Oshima H, Oshima M, Kai K, Torii R, Masuko T, et al. CD44+ slow-cycling tumor cell expansion is triggered by cooperative actions of Wnt and prostaglandin E2 in gastric tumorigenesis. Cancer Sci 2010;101:673–8.
40. Dinarello CA. Why not treat human cancer with interleukin-1 blockade? Cancer Metastasis Rev 2010;29:317–29.